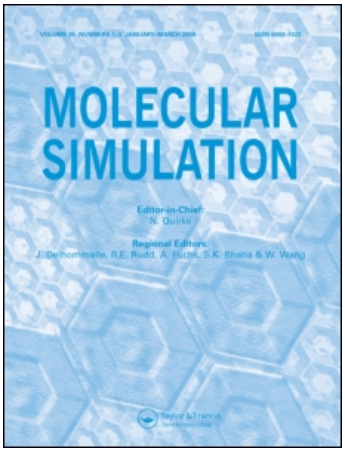


**Molecular Simulation**
Publication details, including instructions for authors and subscription information:
http://www.informaworld.com/smpp/title~content=t713644482

# Computational Soft Nanotechnology with Mesodyn

J. G. E. M. Fraaije[a]; A. V. Zvelindovsky[a]; G. J. A. Sevink[a]
[a] Soft Condensed Matter Group, Leiden Institute of Chemistry, Leiden University, RA Leiden, The Netherlands

**To cite this Article** Fraaije, J. G. E. M. , Zvelindovsky, A. V. and Sevink, G. J. A.(2004) 'Computational Soft Nanotechnology with Mesodyn', Molecular Simulation, 30: 4, 225 — 238
**To link to this Article: DOI:** 10.1080/08927020310001659133
**URL:** http://dx.doi.org/10.1080/08927020310001659133

*Molecular Simulation*, VOL. 30 (4), 15 April 2004, pp. 225–238

Taylor & Francis
Taylor & Francis Group

# Computational Soft Nanotechnology with Mesodyn

J.G.E.M. FRAAIJE*, A.V. ZVELINDOVSKY and G.J.A. SEVINK

*Soft Condensed Matter Group, Leiden Institute of Chemistry, Leiden University, P.O. Box 9502, 2300 RA Leiden, The Netherlands*

*(Received July 2003; In final form October 2003)*



**The simulation of microstructures on a scale 1–1000 nm is a typical problem in colloid and polymer science, and this is also the realm of modern computational "soft nanotechnology". Accordingly, computational methods rely heavily on time-honoured approaches for calculating the thermodynamical stability of complex mixtures. We describe such approaches in the framework of MesoDyn, a general purpose software package for field-based simulations methods, such as the polymer mean-field model for microphase formation and the Poisson–Boltzmann model for electrostatic interactions. The paper concludes with a small review of examples of application: the formation of microscopic structures in block copolymer bulk solutions, block copolymer melt structures on surfaces (thin films) and structure formation in tiny polymer surfactant droplets (polymersomes). The method works quite well in all cases where a mean-field model is appropriate, but it is a challenge to extend the simulations to systems in which specific correlations are important.**

*Keywords*: Mesodyn; Nanotechnology; Simulations; Microstructures

## INTRODUCTION

Mesodyn provides a general framework to calculate the dynamics of mesoscale pattern formation, on a coarse-grained scale 1–1000 nm, in a variety of block polymer mixtures and solutions, including charged systems and systems containing hard particles such as colloids or surfaces. Mesodyn was originally developed at Akzo Nobel in the early 1990s, in an attempt to solve a stability problem in waterborne coatings. Since then, it has been greatly expanded to cover many different systems and external conditions, following two large industrial European research projects, CAESAR and Mesodyn, led by BASF.

The stability problem in waterborne coatings is typical for microscopically structured systems in a traditional industrial setting. Such coating contains various colloids (pigments, fillers) of various sizes and surface properties, in addition to a complex mixture of heterodisperse copolymers and solvents. After setting, the coating is frozen-in into a microstructure which is, more often than not, extremely ill-defined, ill-controlled and very much dependent of the exact procedure by which the coating was applied. In contrast, in the modern approach to soft nanotechnology one seeks systems and procedures, such that the microstructure is precisely controlled, and precisely defined, but still on a production scale large enough to be of potential interest to industry. Accordingly, simulations methods such as Mesodyn can be used to find such systems and conditions.

When one explores the formation of soft objects on a nanoscale, in general the constituents are of two kinds: assemblies of (flexible) block copolymers, and embedded hard particles. The rules for phase separation in such systems must be studied carefully. When homopolymers and solvents or other polymers are mixed the usual situation is a macroscopic phase separation into a dilute and concentrated polymer solution. Such macrophase separation is almost always a nuisance, and ways are sought to avoid it from happening. On the other hand, when one uses (block) copolymers, instead of homopolymers, the system may phase separate internally—this is microphase separation—and form a mesoscale pattern, with typical length scale 1–1000 nm. Morphologies formed include: a distribution of micelles, lamellae, or cylinders, or more exotic structures such as vesicles and bicontinuous phases. These structures may be used to form soft nanoscale objects in large quantities.

*Corresponding author. E-mail: j.fraaije@chem.leidenuniv.nl

ISSN 0892-7022 print/ISSN 1029-0435 online © 2004 Taylor & Francis Ltd
DOI: 10.1080/08927020310001659133

Almost every day, academic and industrial colloid and polymer scientists find examples of new block copolymer morphologies, and investigate possible new applications. The applications vary just as much as the systems: from traditional high-impact polymer materials to novel high-performance elastomers, to advanced drug-delivery polymer capsules and biochips, artificial skin and smart gels, contact lenses and electro-optical polymer displays.

Without exception, in all practical applications of block copolymers and block copolymer solutions, the mesoscale pattern determines the performance. The dynamical pathway of formation is also of crucial importance in almost all of these systems, since the systems easily become trapped in local free energy minima. The dynamics of the patterns are very sluggish: the typical time scale for formation, or change in performance upon shift in conditions, is at least of the order of seconds, if not much larger. The large length and time scales are typical for problems in colloid and polymer science, but they are very large compared to typical motions on molecular scales. Molecular simulations with atomic force fields can be applied to those cases where one has a good idea of the morphologies, and is interested in a "sub-mesoscale" molecular structure, embedded in the mesoscale scaffold; but otherwise the simulation method must be adapted to reach the mesoscale. This is where Mesodyn comes in. It is optimised to do just one thing: the dynamic calculation of the polymer morphology, given all kinds of external conditions and surface interactions. It has guaranteed proper thermodynamic behaviour (in the mean field Flory–Huggins framework), using realistic and readily available parameters such as Flory–Huggins $\chi$ parameters, monomer charge, polymer chain architectures and mixture composition.

The language of Mesodyn is that of traditional colloid and polymer theory, and differs in some important respects from the typical framework of molecular simulations. One now has free energy models, rather than molecular Hamiltonians; coarse-grained interaction parameters rather than force field parameters, concentration variables rather than atomic position variables, and some invented hydrodynamic or diffusion scheme for updating dynamical variables in time. Mesodyn merges two classical theories: the Flory–Huggins theory for polymer phase diagrams, and the Ginzburg–Landau model for dynamic pattern formation.

Hamley's book [1] contains an extensive list of references to morphologies in block copolymer systems, and mean field calculations, and we refer to this book for general information. Here we focus exclusively on the work done in our own group [2,3]. General introductory books are those of de Gennes [4] and Doi and Edwards [5]. An excellent recent review paper dealing with dynamical field models is also available [6].

In the theory section we summarise the continuum Flory–Huggins theory for inhomogeneous solutions and the dynamical equations. In the applications section we present a few examples of morphology calculations in polymer surfactant solutions, block copolymer thin films and polymer surfactant "nano" gels.

## THEORY

### Principle

The classic Flory–Huggins theory is derived based on a lattice model for polymer configurations [7–9]. It is a so-called mean field model in which all thermodynamic properties are calculated from the behaviour of a single polymer chain in the average interaction field generated by its neighbours. The mean field approach is restricted in its application to relatively flexible polymers in concentrated solution and melts, but nevertheless has been applied with tremendous success to a wide variety of phase separation problems.

It is illustrative to recall when and why a single chain mean field model gives a realistic picture of a polymer system. In a dense homogeneous solution of flexible polymer, each chain will sample a number of configurations in a certain volume much larger than the atomic volume of all monomers of the same chain combined. Thus, many chains penetrate the volume element of the coil. When the number of chains in the volume element is very large, the monomer–monomer interactions are uncorrelated from the chain–chain interactions, and the chain generating the coil behaves as if it is embedded in the average field from the other chains.

In an inhomogeneous polymer system, the same argument applies. For example, imagine a triblock copolymer tethered in space by two adjoining micelles in a concentrated solution, as shown in Fig. 1.

In one illustrated case, the polymer surfactant is a "reverse" surfactant, $P_5E_9P_5$, with the hydrophobic blocks at the two ends of the polymer. The two hydrophobic blocks stick in two different micellar cores, and the hydrophilic middle block binds the two micelles together. Such a system would be a good example of a reversible polymer surfactant gel [10]. It will probably be very viscous and on a short time scale even strongly elastic. Such gels find many applications in personal and health care products as slow-release agents, since the micellar cores may act as reservoirs for small organic drug molecules. Notice that the "regular" surfactant with sequence hydrophilic–hydrophobic–hydrophilic

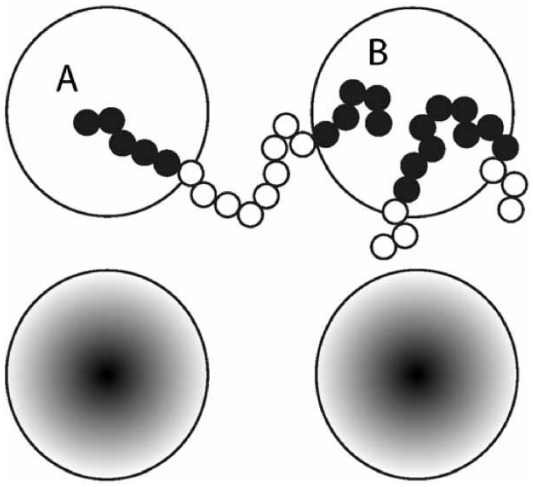


FIGURE 1 *Top*: Micelles of reverse $P_5E_9P_5$ and regular $E_3P_9E_3$ triblock polymer surfactant. Hydrophobic (*P*, black) and hydrophylic (*E*, open) beads indicated. *Bottom*: concentration field of hydrophobic blocks.



(model for Pluronic L64, $E_3P_9E_3$, see "Applications" section) cannot physically connect two micelles, and thus such a gel will be much less viscous or elastic—or will not behave like a reversible gel at all.

In the illustrated micellar system, each polymer molecule is obviously constrained in sampling the conformations compared to an ideal homogeneous system, because of the tethering in space. If the constraints are very strong, only a few conformations will remain, and the mean field picture will break down. But nevertheless in almost all of these applications the interactions are weak, the gel is soft and fragile, enough of the coil volume remains open for other chains and solvent, and the mean field will still be a very good approximation.

It is not trivial to decide from a given detailed molecular architecture if and when a single chain mean field is reasonable or not, and only rough guidelines can be given: (1) the concentration of the polymer should be above the overlap concentration, (2) the polymer must be flexible, so that the coil volume does not deviate too much from that of a random coil, and (3) the coil must be large enough, otherwise too few of the neighbouring chains can penetrate the coil volume element. For example, a dilute solution of short and stiff oligo-carbohydrate molecule with 10 monomers falls (very far) outside the range of applicability of the mean field model. A concentrated solution of low molecular weight surfactants or lipids will also be outside the range of applicability (although less than the previous example), because the chains are too short. A concentrated solution of flexible polymer surfactant, a porous layer of weakly charged polyelectrolyte, or a melt of copolymer will do fine.

### Field Model

The thermodynamic model inherent in Mesodyn is a 3D continuum extension of the Flory–Huggins model. This implies that, if proper limits are taken, the classical mean field behaviour is exactly reproduced. But the details of the model are slightly different. We do not impose the lattice restriction, and the system is not necessarily in equilibrium. Consider again the system in Fig. 1. We imagine that we follow the micelles during a certain period of time by a suitable microscope. The microscope has high enough spatial resolution, so we can see the individual micelles as a concentration field image (like the greyscale micelles images at the bottom in Fig. 1). The collective dynamics of the micelles will be extremely sluggish with a typical collective correlation time of at least a few seconds (depending of course on molecular compositions), much larger than the internal chain relaxation time $\tau_C$. The key assumption in the Mesodyn approach is that on the coarse grained time-scale with time-increment $\gg \tau_C$, all chains sample all possible conformations with proper statistical Boltzmann weight; that is the chains are in local equilibrium. Effectively, the micelles form a slowly changing external potential $U(\mathbf{r})$ such that, given the instantaneous distribution of the micelles in space, the free energy is minimal. From the Boltzmann weight one can calculate all interesting parameters: the entropy, correlation functions and so on, provided of course one knows $U(\mathbf{r})$. But the potential can be calculated by iteration. From the Boltzmann weights one can calculate the average polymer concentration, or monomer concentration profiles. In turn, since the micelles themselves are composed of polymer, the micellar distribution is also determined from the same Boltzmann distribution by proper addition of weights. Thus we have a so-called consistent field method: the spatial distribution of the micelles generates $U(\mathbf{r})$, which generates the Boltzmann weight, which generates the monomer distribution, which generates the micellar distribution, etc. When the set of weights is consistent, that is, when the generated concentration fields exactly match those of the micellar pattern, one can calculate the partition function $\phi$ and related properties through statistical thermodynamics. For example, the concentration field and external potential are related through the derivative of the partition function

$$\rho_I(\mathbf{r}) = -nkT\frac{\delta \ln \phi}{\delta U_I(\mathbf{r})} \tag{1}$$

where $n$ is the number of chains and $I$ the index for the bead type. In the Boltzmann weight calculation, we neglect the inter-chain correlations, since we assume that the mean field governs the intermolecular energetic interactions. The net free energy is

the sum of the ideal free energy for the collection of all types $i$ of single chains, and the mean field contribution:

$$F = -kT\sum_i \ln \frac{\phi_i^{ni}}{n_i!} - \sum_I \int_V \mathrm{d}\mathbf{r}\, U_i \rho_I(\mathbf{r}) + F_{MF} \qquad (2)$$

where $i$ counts the different types of polymer chains, and $I$ the different bead types, $I \geq i$. For example, in a mixture of a block copolymer $AB$ and solvent $C$, $i = AB, C$ and $I = A, B, C$.

The system is not necessarily in global equilibrium. The Boltzmann weight calculation only generates the proper potential, conjugate to the concentration field, and therefore only takes into account the entropy loss due to the confinement in the micelles. It may be that energy can be gained, for example by turning the micelles into cylinders, or perhaps the energy is lower when the inter-micellar distance is made smaller. Global equilibrium is reached only in a stationary state, such that any infinitesimal change in concentration field results in an exact balance of energy and entropy, gain and loss. In a mathematical sense, there are infinitely many small changes $\delta\rho_I(\mathbf{r})$ in the concentration field possible. Some shifts will correspond to a shape change of the micelles; others will lead to a reduction in inter-micellar distance. The net free energy change is:

$$\delta F = \sum_I F[\rho_I(\mathbf{r}) + \delta\rho_I(\mathbf{r})] - F[\rho_I(\mathbf{r})] \qquad (3)$$

$$= \sum_I \int_V \mathrm{d}\mathbf{r} \frac{\delta F}{\delta \rho_I(\mathbf{r})} \delta\rho_I(\mathbf{r}) \qquad (4)$$

$$\frac{\delta F}{\delta \rho_I(\mathbf{r})} = -U_I(\mathbf{r}) + \frac{\delta F_{MF}}{\delta \rho_I(\mathbf{r})} \qquad (5)$$

$$\frac{\delta F}{\delta \rho_I(\mathbf{r})} = 0 \quad \forall I : \text{global equilibrium} \qquad (6)$$

$$\frac{\delta^2 F}{\delta\rho_I(\mathbf{r})\delta\rho_J(\mathbf{r}')} > 0 \quad \forall I, J : \text{stable minimum} \qquad (7)$$

The intrinsic chemical potential is denoted by the functional derivative $\delta F/\delta\rho_I(\mathbf{r})$. It is easy to see that any shift $\delta\rho_I(\mathbf{r})$ with the same sign as $\delta F/\delta\rho_I(\mathbf{r})$ (component wise), leads to an increase in free energy, and thus cannot be the result of an internal spontaneous process. On the other hand, when the shift is the result of a flux, in accordance with the laws of linear nonequilibrium thermodynamics, it will reduce the free energy. For example, for a system with one component, when the flux $\mathbf{J} = -L\nabla\delta F/\delta\rho$, with $L$ a number $>0$, in a small time step $\delta t$, $\delta\rho = \delta t L \nabla^2 \delta F/\delta\rho$ (conservation of mass), then the free energy change is $\delta F = \delta t L \int_V \mathrm{d}\mathbf{r} \delta F/\delta\rho \nabla^2 \delta F/\delta\rho$, and with Gauss theorem neglecting surface integrals $\delta F = -\delta t L \int_V \mathrm{d}\mathbf{r} [\nabla \delta F/\delta\rho]^2 < 0$. The same argument applies to the more elaborate diffusion models listed below.

In global equilibrium with stable minimum, the gradients of the intrinsic chemical potential are zero, and any second order perturbation must lead to an increase in free energy, so that the derivative matrix $\delta^2 F/\delta\rho_I(\mathbf{r})\delta\rho_J(\mathbf{r}')$ must be positive definite. Notice that there are very many such minima possible; almost all of them will be metastable—except for the global minimum, the morphology with the lowest free energy. But this morphology is very difficult to achieve, and the system rather becomes trapped in a metastable state.

## Details of the Free Energy Model

In the equilibrium limit $\delta F/\delta\rho_I = 0$ corresponds exactly to the set of equations of equilibrium polymer self-consistent field models. The equilibrium mean field models come in many flavours: the models have been reinvented several times, in different scientific disciplines. One can perform calculations analytically (known as the Random Phase Approximation, or RPA) [4,11], numerically with a lattice chain model (Scheutjens–Fleer), with a molecular detailed single chain Hamiltonian [13], or numerically with discrete Gaussian chains (Mesodyn) or continuous wormlike chains [14]. The earliest well documented numerical analysis of the self-consistent field model is due to Helfand, in the early 1970s, originally applied to block copolymer layers and polymer blend interfaces [15–17]. In Helfand's model too, the chain is represented as a wormlike continuous chain. The difference between all these models is to a large extent irrelevant. For long enough chains they are all identical, for short chains none of them will apply. There are some differences in ease of use. The analytical RPA approach is the "bread and butter" of polymer physics—if one is well versed in field theory the method can be applied with advantage. The language of the Scheutjens–Fleer lattice chain model is very close to that of the original Flory–Huggins model: one imagines polymers as walks on a regular lattice. The Scheutjens–Fleer model has been applied very successfully to numerous problems in polymer adsorption in colloid and surface science [12].

The discrete Gaussian chain model (Mesodyn) and the continuous chain model only differ in minor details of the Boltzmann weight calculations; both of them have been applied primarily to melts and concentrated solution in bulk. In Mesodyn, a chain is represented as a necklace of beads, each bead representing a large number of monomers. Each bead is thought to be a tiny random coil; the beads are connected via harmonic springs. In the continuous chain model, the chain is a flexible worm, also with harmonic springs between consecutive chain elements.

The details of the model are as follows. The chain Hamiltonian for the necklace of beads is

$$H = \frac{3kT}{2a^2}\sum_{s=2}^{N}(\mathbf{R}_s - \mathbf{R}_{s-1})^2 \tag{8}$$

with $a$ the bead size. Notice that the average distance between consecutive beads is zero: each bead is a tiny coil, and thus can be penetrated by monomers from the adjacent bead. The partition function $\phi$ of a single chain is

$$\phi[U] = \mathcal{N}\int_{V^N} \mathrm{d}\{\mathbf{R}\}\, e^{-\beta\left[H+\sum_{s=1}^{N} U_s(\mathbf{R}_s)\right]} \tag{9}$$

$$\mathrm{d}\{\mathbf{R}\} \equiv \prod_{i=1}^{N}\mathrm{d}\mathbf{R}_i \tag{10}$$

with $\mathcal{N}$ a normalisation constant such that $\phi(0) = V/\Lambda^3$ (ideal gas limit), and $\beta \equiv 1/kT$. The density functional for bead type $I$ of the chain is the ensemble average of a microscopic density operator

$$\rho_I[U](\mathbf{r}) = \sum_{x=1}^{N}\theta_{Ix}\rho_x(\mathbf{r}) \tag{11}$$

$$\rho_x(\mathbf{r}) = n\langle\delta(\mathbf{r}-\mathbf{R}_x)\rangle \tag{12}$$

$$\langle\delta(\mathbf{r}-\mathbf{R}_x)\rangle = \frac{\int_{V^N}\mathrm{d}\{\mathbf{R}\}\delta(\mathbf{r}-\mathbf{R}_x)e^{-\beta\left[H+\sum_{s=1}^{N}U_s(\mathbf{R}_s)\right]}}{\int_{V^N}\mathrm{d}\{\mathbf{R}\}e^{-\beta\left[H+\sum_{s=1}^{N}U_s(\mathbf{R}_s)\right]}} \tag{13}$$

where $\theta_{Ix}=1$ when bead $x$ is of type $I$, and 0 otherwise.

At the heart of all ideal chain models is an efficient algorithm for the calculation of the partition function and concentrations fields. The algorithm is either called the matrix scheme (in 1D lattice theories), and/or propagator scheme (for discrete chains in continuum), or Edwards diffusion equation (continuous chains in continuum). The algorithm uses the phantom character of the ideal chain. Any point along the chain, somewhere in space, can be regarded as the product of two weighted random walks, one in the direction from $1 \rightarrow N$, and the inverse from $N \rightarrow 1$. For example, for the discrete chain we define the recurrence relations for propagator functions $G$ and $G^i$

$$G_s(\mathbf{r}) = e^{-\beta U_s(\mathbf{r})}{}_{\sigma[G_{s-1}](\mathbf{r})} \quad s: 1 \rightarrow N \tag{14}$$

$$G_s^i(\mathbf{r}) = e^{-\beta U_s(\mathbf{r})}{}_{\sigma[G_{s+1}^i](\mathbf{r})} \quad s: N \rightarrow 1 \tag{15}$$

$$G_0(\mathbf{r}) = 1 \tag{16}$$

$$G_{N+1}^i(\mathbf{r}) = 1 \tag{17}$$

with the linkage operator as a Gaussian filter

$$\sigma[f](\mathbf{r}) = \left(\frac{3}{2\pi a^2}\right)^{\frac{3}{2}}\int_V \mathrm{d}\mathbf{r}'\, e^{-\frac{3(\mathbf{r}-\mathbf{r}')^2}{2a^2}} f(\mathbf{r}') \tag{18}$$

It is not difficult to see that

$$\phi\Lambda^3 = \int_V \mathrm{d}\mathbf{r}\, G_N(\mathbf{r}) \tag{19}$$

$$= \int_V \mathrm{d}\mathbf{r}\, G_1^i(\mathbf{r}) \tag{20}$$

$$\rho_s(\mathbf{r}) = n\frac{G_s(\mathbf{r})\sigma[G_{s+1}^i](\mathbf{r})}{\int_V \mathrm{d}\mathbf{r}\, G_N(\mathbf{r})} \quad \text{composition law} \tag{21}$$

It is apparent from the recursion that the computational cost of a calculation scales linearly with the length of the chains: double the chain length, and the calculation of the partition function is twice as expensive. These recurrence relations are crucial for efficient numerical evaluations, but otherwise do not affect the thermodynamics.

The mean field free energy is a sum of separate mean-field interactions: bead–bead ($F_{\mathrm{BB}}$) and bead–surface interactions ($F_{\mathrm{BM}}$), compressibility interactions ($F_{\mathrm{C}}$), electrostatic interactions ($F_{\mathrm{el}}$), and bead-auxiliary field inter-actions ($F_{\mathrm{Bf}}$)

$$F_{\mathrm{MF}} = F_{\mathrm{BB}} + F_{\mathrm{C}} + F_{\mathrm{BM}} + F_{\mathrm{el}} + F_{\mathrm{Bf}} \tag{22}$$

The bead–bead interaction is quadratic:

$$F_{\mathrm{BB}} = \frac{1}{2}\sum_{IJ}\int_V\int_V \mathrm{d}\mathbf{r}\,\mathrm{d}\mathbf{r}'\,\epsilon_{IJ}(\mathbf{r}-\mathbf{r}')\rho_I(\mathbf{r})\,\rho_J(\mathbf{r}) \tag{23}$$

with Gaussian interaction kernel, of the same width as the bond length in the chain

$$\epsilon_{IJ}(\mathbf{r}-\mathbf{r}') \equiv \epsilon_{IJ}^0\left(\frac{3}{2\pi a^2}\right)^{\frac{3}{2}} e^{-\frac{3(\mathbf{r}-\mathbf{r}')^2}{2a^2}} \tag{24}$$

In RPA one usually takes a local interaction model, but in lattice models as well as here, one takes a weighted average over neighbour interactions. The nonlocality is especially important if one is interested in phenomena on the small scale of the beads: since in the model the beads are penetrable coils, the interaction must necessarily be spread on the scale of the bead.

The compressibility term (originally due to Helfand) allows for small (harmonic) deviations of a few per cent from average total density—the system is thus slightly compressible which has some advantages for the numerical calculations:

$$F_C = \frac{\kappa}{2}\int_V \mathrm{d}\mathbf{r}\left(\sum_I \nu\rho_I(\mathbf{r}) - 1\right)^2 \tag{25}$$

The mean field excluded volume parameter is $\nu$, the compressibility parameter $\kappa$. It is also possible to adjust the free energy such that the system is exactly incompressible, by including an additional constraint via a Lagrange multiplier, through $F_C = \int_V \mathrm{d}\mathbf{r} p_L(\mathbf{r})\left(\sum_I \nu\rho_I(\mathbf{r}) - 1\right)$, where $p_L$

(sometimes confusingly referred to as a pressure) is the additional multiplier. In many other self-consistent-field models this approach is taken, but we have abandoned it, since the compressible models is much easier to work with—and also more physical. The bare interactions are related to the dimensionless Flory–Huggins $\chi$-parameters through

$$\chi_{IJ} = \frac{\beta}{2\nu}(\epsilon^0_{II} + \epsilon^0_{JJ} - \epsilon^0_{IJ} - \epsilon^0_{JI}) \tag{26}$$

For the electrostatic free energy one can use any type of electrostatic interaction (Debye–Hückel, Poisson–Boltzmann, Donnan, etc.), as long as the interaction is on the level of mean-field. For example, in the case of a Donnan model one assumes that locally, on a coarse grained scale, each "cell" or point in space is electroneutral. The electrostatic free energy is then just the mixing free energy of the neutral salt. For a system with 1–1 electrolyte in equilibrium with a neutral salt bath of concentration $c_s$, the electrostatic free energy is the excess with respect to the bath:

$$F^{\text{Donnan}}_{\text{el}} = kT\sum_{\alpha=+/-}\int_V \mathrm{d}\mathbf{r} c_\alpha[\ln\frac{c_\alpha}{c_s} - 1] + \int_V \mathrm{d}\mathbf{r}\lambda_D(\mathbf{r})Q(\mathbf{r}) \tag{27}$$

with $c_\alpha(\mathbf{r})$ the local concentration of ion $\alpha$ (+ or −), $\lambda_D(\mathbf{r})$ the Donnan potential, and $Q$ the local charge density (in units of $e$): $Q(\mathbf{r}) \equiv \sum_{\text{beads}} z_I\rho_I + \sum_{\alpha=+/-} z_\alpha c_\alpha$. The Donnan potential is determined from the condition that the local charge density is zero $Q(\mathbf{r})=0$. Such a model applies well when the salt strength is high and/or the polymer charges are low. Similar models can be used for Debye–Hückel or Poisson–Boltzmann, in which case one needs to replace $\int_V \mathrm{d}\mathbf{r}\lambda_D Q$ by the free energy stored in the electric field $1/2\int \mathrm{d}\mathbf{r}\epsilon\mathbf{E}^2 + \int \mathrm{d}\mathbf{r}4\mathrm{Q}$.

The interactions with surfaces of embedded particles are modelled in the same spirit, where we borrow a simple concept from image processing to define the surface layer [18]. One imagines a collection of hard particles of certain geometry in the system, described by a boolean mask field $M(\mathbf{r})$. On the inside of a particle $M = 0$, outside $M = 1$. From the mask field, one can calculate several geometrical properties, for example, the total volume of the particles is obviously $\int_V \mathrm{d}\mathbf{r}M(\mathbf{r})$. The surfaces of all the particles in space can be traced by convolution of the inverse mask $\bar{M} \equiv 1 - M$ with a mask smoothing Gaussian kernel $\sigma_M = (3/2\pi\mathrm{d}^2)^{3/2} \times \int \mathrm{d}\mathbf{r}' \exp[-3(\mathbf{r} - \mathbf{r}')^2/2\mathrm{d}^2](\bullet)$

$$S(\mathbf{r}) \equiv M\sigma_M\bar{M} \tag{28}$$

$S(\mathbf{r})$ is in itself also a field in 3D, narrowingly following the contours of the hard particles with a thin layer (like a glove on a hand), with width determined by the length $d$ of the mask kernel $\sigma_M$. Several choices for $\sigma_M$ can be made: in the presented applications (thin films) we used the same Gaussian kernels as for the bead–bead interactions $d = a$. Knowing the surface layer, one can easily add the interactions. For example, in case of a homogeneous surface

$$F_{\text{BM}} = \sum_I \epsilon^0_{\text{IM}} \int_V \mathrm{d}\mathbf{r}\rho_I(\mathbf{r})S(\mathbf{r}) \tag{29}$$

with $\epsilon^0_{\text{IM}}$ a bead-mask interaction parameter.

Finally, for some applications one is interested in calculating the effect of an applied auxiliary potential. Such potential need not be physical. For example, in the processing of experimental data from AFM or EM, one wishes to interpret 2D pictures in terms of the underlying 3D structures. These are so-called inverse-mapping problems, leading to a formulation in a thermodynamic-informatics model. A simple way to do so is to recast the experimental information in an auxiliary potential or penalty function. The interaction model depends in this case very much on the particular application one has in mind. Suppose one has knowledge of the concentration profile $\rho^{\text{exp}}_I(\mathbf{r})$, in a certain subdomain $\Omega$. In the spirit of the maximal uncertainty method, one then constructs an auxiliary free energy term (or constraint)

$$F_{\text{Bf}} = \int_\Omega \mathrm{d}\mathbf{r}\lambda_{\text{Bf}}(\mathbf{r})\big(\rho_I(\mathbf{r}) - \rho^{\text{exp}}_I(\mathbf{r})\big) \tag{30}$$

with $\lambda_{\text{Bf}}$ an additional Lagrange multiplier. The extremum of $F$ (a saddlepoint with respect to $\rho_I$ and $\lambda_{\text{Bf}}$) now determines the least biased 3D reconstruction, given the known profile $\rho^{\text{exp}}_I$ in the subspace $\Omega$. Examples of diblock copolymer morphology reconstruction following this method have been published [19], but are not discussed further here.

So far, the presented free energy model is suitable for flexible polymers in a mean field. The extension to stiff-flexible polymers is possible, by invoking additional tensorial order parameters for average bond directions [20]. For example, the average of the inner-product of the bonds between bead $s$ and $s + 1$, and $s - 1$ and $s$ is

$$T_{s,\alpha\beta} \equiv n\langle\delta(\mathbf{r} - \mathbf{R}_s)(\mathbf{R}_{s,\alpha} - \mathbf{R}_{s-1,\alpha})(\mathbf{R}_{s+1,\beta} - \mathbf{R}_{s,\beta})\rangle \tag{31}$$

with $\alpha, \beta = x,y,z$. The model introduces the tensorial external potential $\mathbf{W}$ conjugate to $\mathbf{T}$, through a bond–bond interaction which is added to the chain Hamiltonian $H = H^0 + \sum_s(\mathbf{R}_s - \mathbf{R}_{s-1}) \times \mathbf{W}_s \times (\mathbf{R}_{s+1} - \mathbf{R}_s)$. Unfortunately, the bond–bond interaction disrupts the simple recursion scheme for the chain propagators, and now the scheme requires repeated 6D integration rather than the repeated 3D integration applicable to flexible polymers. The cited numerical results have only recently

been obtained for block copolymers in 2D systems [20], but these results already indicate stiffness is a very important control parameter for the microphase formation.

### Dynamics

The dynamical model is that of convection-diffusion. By assumption, on the coarse-grained time scale the chain distribution function is relaxed constantly, since all internal modes are in equilibrium. The simplification is enormous, since now we do not have to consider memory effects associated with unrelaxed chain conformations. In fact, we simply combine the flux equations of linear nonequilibrium thermodynamics

$$\begin{aligned} \text{Diffusion}: \quad & \mathbf{J} = -L\nabla\frac{\delta F}{\delta\rho} \\ \text{Convection}: \quad & \mathbf{J} = \mathbf{v}\rho \end{aligned} \tag{32}$$

($L$ is a positive definite Onsager coefficient and $\mathbf{v}$ the velocity field), with the law for the conservation of mass

$$\frac{\partial\rho}{\partial t} + \nabla\mathbf{J} = 0 \tag{33}$$

At this point, we do not yet consider hydrodynamics: in the example below where we shear a morphology, the velocity field is imposed from the outside. For most mesoscale polymer systems considered by the molecular modelling community, relaxation by internally driven hydrodynamics is relatively unimportant. Also, it is not easy to find a general purpose model. At this point we do not have a good expression for the local stress; if we do, we can extend the approach better to chemical engineering applications such as extrusion.

There are a few catches to the diffusion model—several models are possible for the Onsager coefficient. In first approximation one can simply set the Onsager coefficient $L$ as a constant, but obviously such models neglect the fundamental property that net flux should be proportional to force and concentration. A slightly better option, therefore, is to take a constant friction coefficient, and set $L = M\rho$ (this is the local coupling or "mixed dynamics" algorithm in Mesodyn). But this approximation is also not entirely consistent, and neglects the extension of the chain. In the inhomogeneous system, each chain samples many conformations, and one should in fact add all thermodynamic forces for each conformation with the proper Boltzmann weight [21,22]. For example, consider again Fig. 1. Suppose micelle A is in equilibrium, so that the intrinsic chemical potential $\delta F/\delta\rho$ is constant in the neighbourhood of A. According to local coupling models the fluxes in A will be zero, since the gradients of the intrinsic chemical potential are zero locally. But now, if micelle B is out of equilibrium and experiences a force in a certain direction, because of the mutual bridging connections micelle A will also experience a force in the same direction, and move accordingly. This effect is captured by the collective Rouse dynamics model, in which the thermodynamic forces are weighed with a long range kernel derived from the monomer-monomer correlations—this is the collective Rouse dynamics or external potential dynamics algorithm in Mesodyn. A similar, but more involved model can be derived for reputation.

$$L = \begin{cases} M & \text{constant} \\ M\rho & \text{local coupling} \\ \int_V \mathrm{d}\mathbf{r}'\Lambda(\mathbf{r}',\mathbf{r})\bullet & \text{general (Rouse, reptation)} \end{cases} \tag{34}$$

The literature on the various dynamical models in not extensive, also very few experimental results are available to check whether it is worthwhile to derive more elaborate models for the Onsager coefficients.

A second catch is the noise. If one observes the movements of a colloidal particle, the Brownian motion will be evident. There may be a constant drift in the dynamics, but the movement will be irregular. Likewise, if one observes a phase separating liquid mixture on the mesoscale, the concentration levels would not be steady, but fluctuating. The thermodynamic mean field model neglects all fluctuations, but they can be restored in the dynamical equations, similar to added noise in particle Brownian dynamics models. The result is a set of stochastic diffusion equations, with an additional random noise source $\eta$ [23]. In principle, the value and spectrum of the noise is dictated by a fluctuation dissipation theorem, but usually one takes simply a white noise source.

Finally, one realises of course that in the compound system all fields of all components interact thermodynamically and dynamically, which is reflected in the choice for the Onsager coefficients and the interaction model. If we now put everything together, we have the general equation

$$\frac{\partial\rho_I}{\partial t} + \nabla\mathbf{v}\rho_I = \sum_J \nabla\int_V \mathrm{d}\mathbf{r}'\Lambda_{IJ}(\mathbf{r}',\mathbf{r})\nabla_{\mathbf{r}'}\frac{\delta F}{\delta\rho_J} + \eta_I \tag{35}$$

## APPLICATIONS

We discuss four illustrative applications from our own work: the phase diagram of a polymer surfactant solution with and without shear, block copolymer thin film formation and microstructure formation in polymer surfactant "nano" droplets.

### Polymer Surfactant Solution

The surfactant in case, L64, is a member of the Pluronic family (marketed by BASF); these are

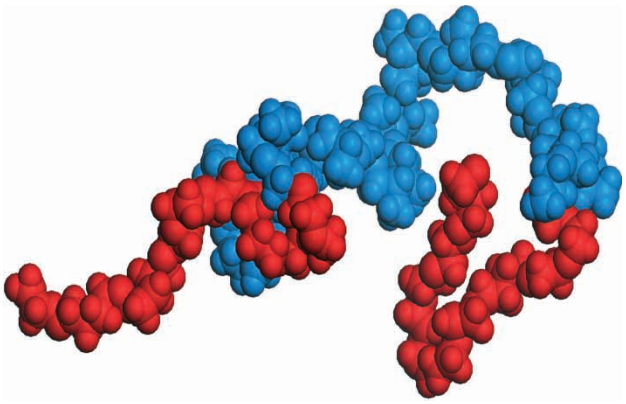

FIGURE 2 Molecular model of Pluronic L64, $(EO)_{13}(PO)_{30}(EO)_{13}$.

triblocks composed of poly(ethyleneoxide) (PEO) and poly(propyleneoxide) (PPO) blocks. Some of these surfactants are popular in drug delivery, others are used in washing powders and personal care products such as toothpaste. The surfactants are "soft"—they are mild to the skin. The amphiphilic power is modest too. The hydrophilic block PEO is only slightly less hydrophobic than the PPO block. In fact the solubility of PEO is an unresolved mystery in itself, possibly related to the cage structure of the hydrated ethyleneoxide monomer.

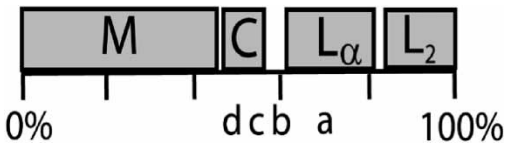


FIGURE 3 Experimental phase diagram of Pluronic L64 in water. Polymer weight fraction indicated. M, Micellar phase; C, Hexagonal (cylindrical) phase; $L_\alpha$, lamellar phase; $L_2$, water-lean continuous phase. Region between M and C: mixed M + C, in between C and $L_\alpha$: mixed $C + L_\alpha + L'$, with L′ bi-continuous. Adapted from Ref. [24]. Labels a–d refer to simulations (Fig. 4).

Polymethyleneoxide is insoluble, PEO is soluble, PPO and polybutyleneoxide and higher are all insoluble. The molecular structure and phase diagram of L64 are shown in Figs. 2 and 3. The triblock polymer is $EO_{13}PO_{30}EO_{13}$, first a hydrophilic block, than a long hydrophobic block and then again the hydrophilic block. The mesoscale simulations proceed by calculating the lyotropic phases in a narrow concentration range 50–70% [24]. From accurate experimental data [25–27], in this interval four phases are known, and the structure factors have been measured: micellar phase, cylindrical or hexagonal phase, a bicontinuous phase and a lamellar phase. The original paper [24] reproduced all important characteristics of

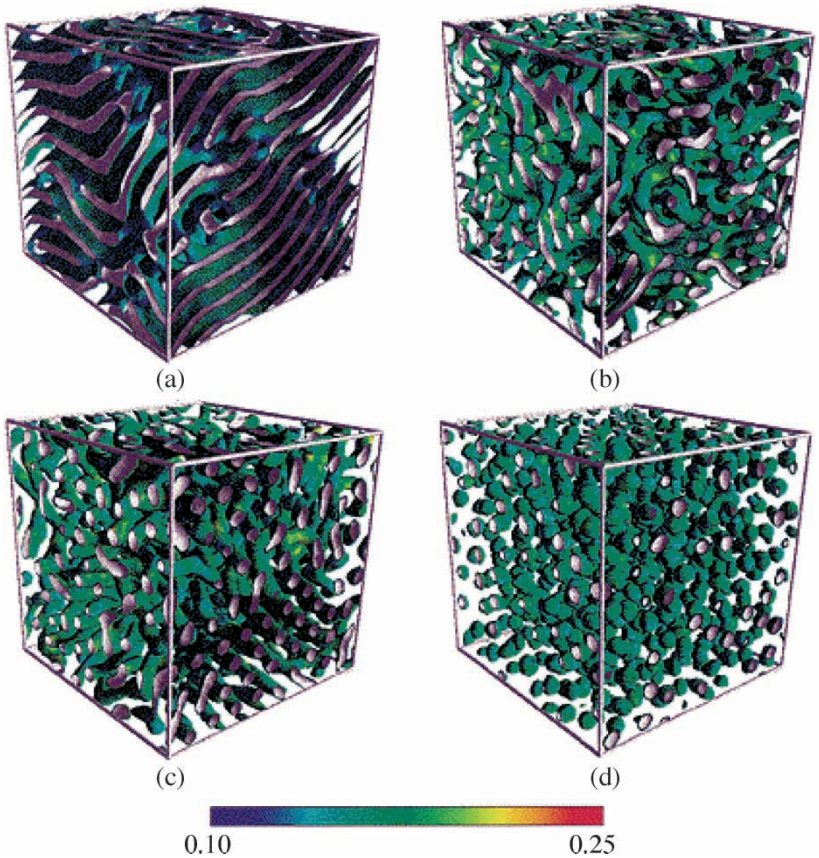


FIGURE 4 Snapshots of mesoscale structures in L64 polymer surfactant solutions at dimensionless time = 4200. PO isosurfaces with EO surface distribution in colour. (a) 70%, isolevel PO = 0.59, (b) 60%, isolevel PO = 0.5, (c) 55%, isolevel PO = 0.46, (d) 50%, isolevel PO = 0.42. EO as indicated in the colour legend. Figure from Ref. [24].

the phases: the lyotropic order, the phase boundaries, the size and the structure factor (Fig. 4). In the presented simulations we started from a homogeneous solution, then quenched the solution to the proper Flory–Huggins values for the inhomogeneous system. During the subsequent collective diffusive relaxation, the free energy goes down and order parameters go up. The indicated results (Fig. 4) are snapshots of the isodensity surfaces of the propyleneoxide monomer concentration at a certain value of dimensionless time, defined by $\tau = k_B TMh^{-2}t$, with $M$ the mobility $h$ the mesh size (related to bead size through $a/h = 1.1543$, for details of numerics see Ref. [3]) and $t$ "real" time.

In the mesoscale modelling, we have addressed the necessary parametrisation issues as follows. First, the molecular model is converted into a representative Gaussian chain. From a practical point of view it is desirable to use as few beads as possible, since the computational cost scales linearly with $N$, but not too few beads, since then we would lose sufficient resolution of the blocks along the chain. For the purpose of the single-chain density calculations a "real" molecular detail polymer chain (such as the model in Fig. 2) can be replaced by a Gaussian chain, provided the response functions (or correlators) are the same. The calculation of response functions for Gaussian chains is easy (and takes only a fraction of a second on a PC), while the correlation calculation for the molecular model is more cumbersome, but nevertheless can be done. In this way, we have found that the linear response curves are indistinguishable if we replace each 3–4 monomers by one Gaussian bead. Thus, the Gaussian chain is determined as E3P9E3, where "E" is an ethyleneoxide bead and "P" a propyleneoxide bead—this is the regular surfactant depicted in Fig. 1. In the theory section, we have remarked that each bead should have a large number of monomers, so that it behaves as a tiny random coil. The small number of monomers per bead we have used here is probably the lower limit of applicability—it would be better to use a larger monomer/bead ratio. By consequence of the physical size of the bead, the solvent is represented by a single particle, with the same excluded volume as the polymer bead, and with unresolved internal structure.

Second, having established the molecular chain, the Flory–Huggins parameters need to be determined. This is not a trivial matter. We remarked already that PEO is a strange polymer, which should be insoluble as member of an insoluble homologous series, but is not. This is reflected in a strong dependence of the molecular interaction parameters on factors such as concentration and temperature, as well as chain length. Recent comparison of molecular dynamics simulation and a thermodynamic model indicates to a strong influence of hydrogen-bond network formation [29], with competition between water–water and ethyleneoxide–water bonds. It is at present a challenge to calculate the Flory–Huggins parameters from first principles (such as molecular modelling or force field models). But fortunately, since PEO (or its cousin PEG and also PPO) is a well-studied polymer, a large body of experimental data is available which allows us to proceed in a semi-empirical fashion. Already, in the early 1950s, Flory–Huggins parameters were calculated from vapour pressure data on PEG and PPO homopolymer solutions [28]. In the concentration interval 50–70%, the $\chi$-parameters are nearly constant, with (for homopolymers of length similar to the blocks in the surfactant) $\chi_{EW} = 1.4$ and $\chi_{PW} = 1.7$. We used here the standard Flory–Huggins expression for the solvent vapour pressure, $\ln p/p^0 = \ln(1-\theta) + (1-1/N)\theta + \chi\theta^2$, with an important twist: rather than inserting $N$ as the number of monomers, as is commonly done, we interpret $N$ as the number of beads. Correspondingly, the effective bead-based $\chi$-parameters are surprisingly high. Interpreted in a naive fashion, it would seem to imply that a very long polymer of the ethyleneoxide monomer is insoluble, in contrast with the common observation that, for example, PEG is soluble in all compositions. But, as we have remarked before, the numbers are semi-empirical and dependent on various factors, including chain length. As a result of the semi-empirical fit, we have a reasonable model for the solvent controlled swelling of the hydrophilic and hydrophobic blocks, and thus the relative domain volumes. It is the ratio of these volumes which determines the particular phase, and is probably the most important factor in getting the right lyotropic phase diagram. We could not find experimental data of similar quality to estimate the E–P bead–bead interaction. Hamley and co-workers [30] determined the Flory–Huggins parameter in a series of melts of diblock poly(ethyleneoxide)–poly(propyleneoxide), through small-angle X-ray scattering, and estimated a low value $\approx 0.1$, on monomer basis (using our monomer/bead ratio 3–4, this would imply $\approx$ 0.3–0.4 on bead basis). However, such an estimate in a melt does not necessarily reflect the effective behaviour in solutions, as we have remarked before. From group contribution methods [31], taking into account the 3–4 monomers in each bead, we roughly estimated the effective Flory–Huggins parameter between beads as 3–5. In the simulation, we used $\chi_{EP} = 3.0$; this is almost an order of magnitude larger than Hamley's finding.

### Polymer Surfactant Solution under Shear

The results agree very well with the established experimental phase diagram, both in the size-scale of the domains as in the detected lyotropic phases.

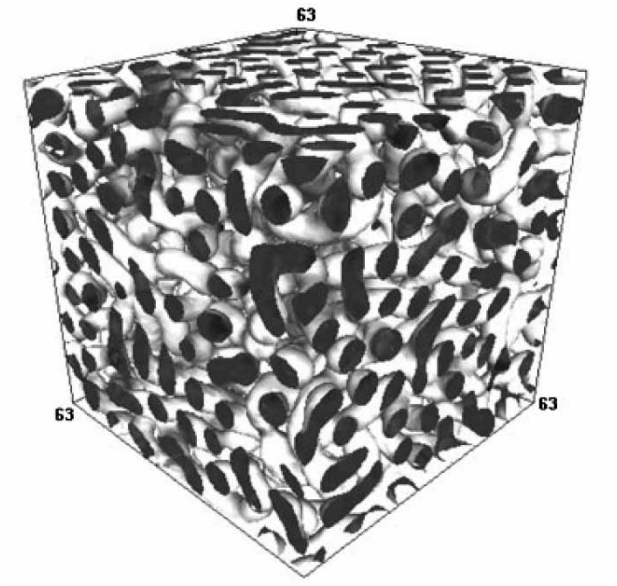


FIGURE 5 Disordered hexagonal phase of 55% L64 solution.

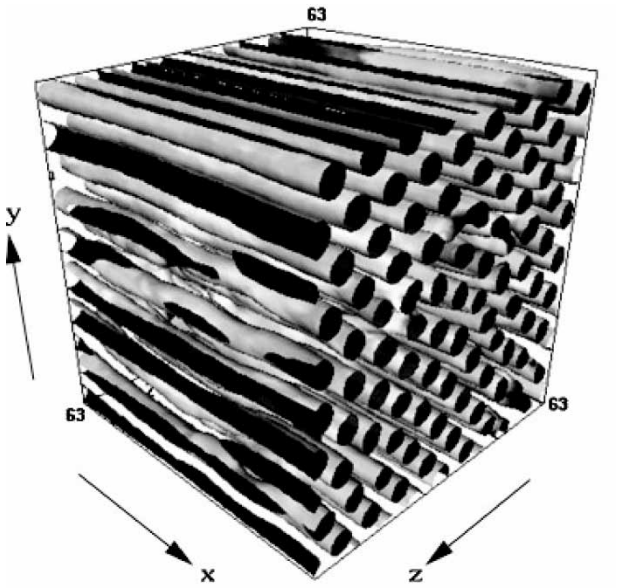


FIGURE 6 Sheared hexagonal phase of 55% L64 solution (Fig. 5).



But the phases are not perfect. Is this also correct? Indeed, also in experimental systems the phases are almost always less than perfect, and ways are sought to apply "external" agents, such as surfaces or shear fields to force the phases into perfect symmetry. Hence, we sheared the L64 hexagonal phase (55%) by adding a directional convective term to the dynamical equations (steady shear). The results (Figs. 5–7, from Ref. [32]) clearly show the adjustment of the microphase to the imposed shear field. From an initial random oriented cylindrical phase, the systems develop into an almost perfect array of hexagons, in the direction of shear. A significant detail is the orientation of the hexagons: they are slightly tilted with respect to the shear gradient. There are several clues in the experimental literature indicating this is indeed correct. In the initial stages of shear, the reordering proceeds via breakup of the structures, which leads to an increase of the anisotropy. The pieces are tilted in the direction of flow. Then oblong micelle-like structures coalescence to form new cylinders which align in the direction of shear. This reorientation is reflected in the rapid increase in the anisotropy factor. The alignment process is clearly observed in the projections of the 3D structure factor. The *yx*-projection is squeezed into a line and the *yz*-projection forms a circle. The position of primary peak remains the same during shearing. The characteristic features of the last stage of reorientation are defect annihilation and reordering of hexagonal clusters. Initially, there are many hexagonal clusters with different orientations. In the final stage, the system forms a few big clusters with nearly the same orientation. Experiments on the same Pluronic surfactant solution [33], with almost the same concentration (53%), demonstrate exactly the same alignment of cylinders in the direction of flow as in our simulation. The 10 planes of the hexagonal lattice is experimentally found to be parallel to the shear plane. Our simulation gives the orientation of the main cluster that is 10° off. For another triblock copolymer system the perpendicular lattice orientation was found together with the same orientation of cylinders along the flow [34].

### Thin Film Formation

In the soft condensed matter literature, an impressive agreement between self-consistent-field theory and experiment was unravelled some time ago by Matsen and Schick [35]. The comparison concerned the microphase diagram of diblock copolymers, with the classical sequence of microphases, depending on block ratio: lamellar, cylindrical and micellar, with gyroid in between lamellar and cylindrical. The microdomain structure in the bulk is determined mainly by the molecular architecture, in particular the ratio of block lengths and the interaction between

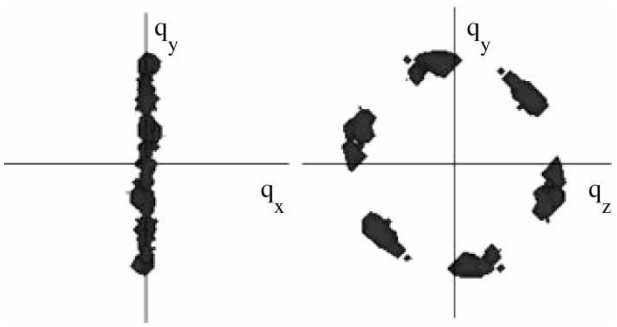


FIGURE 7 Fourier transforms of the sheared hexagonal phase in Fig. 6.

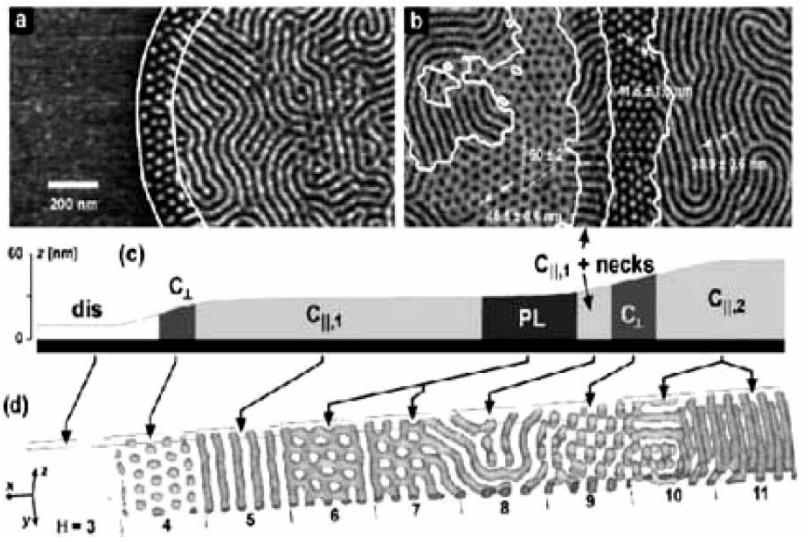


FIGURE 8 A comparison of experiments and Mesodyn simulations. Film with increasing film thickness $H(x)$, $\varepsilon_{AB} = 6.5$, and $M = 6.0$. The latter corresponds to a preferential attraction of $B$ beads to the surface. The isoconcentration surface $\rho_A = 0.5$ is shown. Figure from Ref. [36].



the two components (blocks). At interfaces and in thin films an additional driving force for structure formation exists, because one component typically has a lower interfacial energy than the other. This phenomenon belongs to a class of interfaces of modulated phases, and is specific to the particular system and/or route of film preparation. As a result, no general agreement is reached about the underlying fundamentals. In thin films, additional constraints exist. Here, the microdomain structure has to adjust to two boundary surfaces and a certain film thickness, which can be a noninteger multiple of the natural bulk domain spacing. Both constraints together cause a complex and interesting phase behaviour.

We calculated the microphases of a thin film of neat three block polystyrene–polybutadiene–polystyrene (SBS) deposited on a solid substrate [36]. The parametrisation protocol was somewhat different than in the case of L64, now using data on the microphase separation temperature of a bulk melt to determine the critical Flory–Huggins value, rather than solution data. Figure 8 shows experimental data on morphologies in the thin SBS film, and the comparison with the simulation. Here, the thickness of the simulated block copolymer film was imposed following a gradient in the $x$-direction; in the experimental system steps on the surface with variable thickness were detected and analysed. The agreement between experiment and simulation is very good: a sequence of 9 morphologies is found, in one simulation, in the right order. The sequence runs from from completely disordered very thin films to films with 2 cylinders parallel to the surface, with exotic intermediate structures such as perforated lamellae and perpendicular cylinders.

Well-defined microdomain patterns have formed, which change systematically as a function of the gradually changing film thickness (at steps between terraces). In particular, boundaries between different structures correspond to height contour lines. A major fraction of the surface displays bright stripes, which are indicative of polystyrene cylinders oriented parallel to the surface. In thinner regions of the film, two additional patterns are found: one is characterised by hexagonally ordered dark spots, indicative of polybutadiene microdomains in an otherwise continuous polystyrene layer, i.e. a perforated lamella (PL). The slopes between neighbouring terraces display a hexagonal pattern of bright dots, indicative of polystyrene cylinders oriented perpendicular to the surface (C). Finally, the thinnest parts of the films display no lateral structure at all, indicative of either a disordered (dis) phase or a lamellar wetting layer (W). In thicker films, the sloped regions between terraces display stripes as well. We note that these phases were all reported earlier and for various experimental conditions and cylinder-forming block copolymers. In the present experiments and simulations, however, all phases appear in a single system and under identical experimental conditions. This finding indicates that the film thickness is an important control parameter.

### Polymer Surfactant "nano"droplets

The simulation parameters are for diblock polymer surfactant $A_{N-M}B_M$ with $N = 20$ in weakly selective solvent and mild segregation, $\chi_{AS} = 1.7$, $\chi_{AB}N = 40$, $\chi_{AS} - \chi_{BS} = 0.3$, so that A is slightly more solvophobic and B slightly more solvophilic

(More details are in Ref [37]). These are essentially the parameters we verified before by comparison with experimental microphase diagrams of concentrated polypropyleneoxide–polyethyleneoxide aqueous solutions in ambient conditions [24] (see above), in which case each bead or statistical unit corresponds to 3.4 monomers. One should realise that in the mean-field model any polymer surfactant solution with the same properly scaled interaction parameters will behave in exactly the same way. Here, the diblock polymers are insoluble: the hydrophobic block is so large, that the concentration of unimers in bulk is effectively zero.

The simulations proceed with a sudden quench of a homogenous droplet in a solvent bath. Following the quench, the droplet takes up or releases additional solvent locally and globally, depending on the particular morphology being formed. The polymer concentration outside the droplet is zero, and this remains so during the morphology adaptation. The results are in Fig. 9. The droplets are placed in the centre of the box with sufficient space, $N/2$ cells, between the droplet surface and the boundaries of the computational box, thereby avoiding artefacts resulting from the periodic boundary conditions. In all cases, the droplets develop an outer fuzzy layer of the solvophilic B block, but since the confinement of the polymers is soft, the droplet surface is not necessarily spherical. The surface topography is that of small valleys, ridges and bumps, reflecting the underlying morphology, very much like earth's topography is an image of deeper events. The internal structures, shown in Fig. 9, depend on the size ratio $f = M/N$ similar to bulk block copolymer systems. More symmetric polymers $f = 0.35$ form into an onion structure of alternating A and B layers (Fig. 9a); slightly less symmetric polymers $f = 0.30$–$0.25$ form a bicontinuous phase (Fig. 9b,c), then at $f = 0.20$ a cylindrical phase (Fig. 9d) and an inverted micellar phase (Fig. 9e) at $f = 0.15$. Two asymmetric polymers $f = 0.1$ do not form any internal structure (Fig. 9f). In equilibrium the droplets contain an appreciable amount of solvent (ca. 15%), distributed inhomogeneously over the solvophobic A and solvophilic B rich layers.

In the case of $f = 0.25$, the layers are perforated with pores, and the entire structure is bicontinuous. The droplet strikingly resembles a buckyball, containing in each inner layer a mixed pore pattern of pentagons, hexagons and septagons. In bulk solution or melt systems, perforated lamellae consist ideally of a perfectly hexagonal array of pores. In the curved nanodroplets, by rule of geometry, a perfect array of hexagons is impossible to form, and the perforation is mixed. In bulk, a mixture of 85% of this particular polymer surfactant and 15% solvent forms a gyroid bicontinuous structure (data not shown).

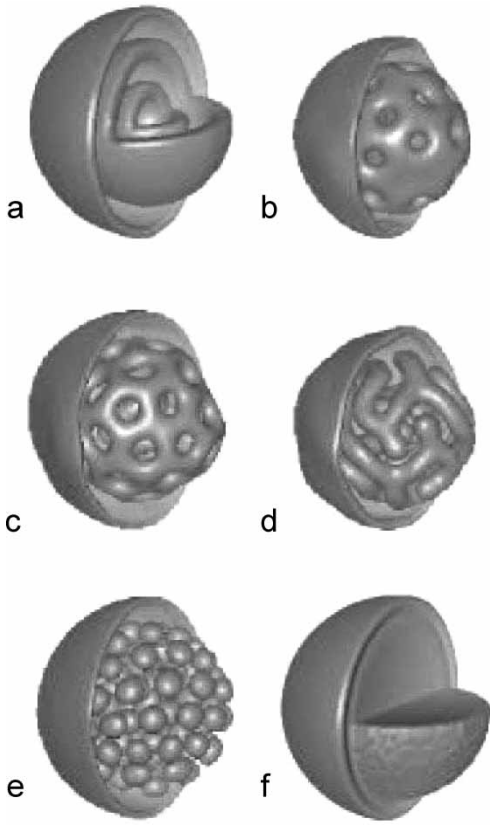


FIGURE 9 Morphologies of $A_{N-M}B_M$ polymer surfactant nanodroplets (iso-surfaces partly removed for visualisation). Solvophobic $A$ concentration field for different block ratios $f = M/N$. 0.35 (a), 0.30 (b), 0.25 (c), 0.20 (d), 0.25 (e), 0.10 (f).

There is no intrinsic magic "60" number, as in $C_{60}$, associated with additional stability of the nanodroplets. The resemblance with a carbon bucky-ball is purely coincidental, based on a geometrical rule for packing pores in a spherical shell.

One may consider several experimental methods for generating the structures—similar as in studies of lipid aggregates—for example, by dispersing insoluble polymer surfactant through sonification, or through destabilizing a suitable surface film. Perforated lamellar or similar bicontinuous structures have been observed experimentally in thin polymer films [36], and in simulations of confined systems [38]. Isolated, closed block copolymer membrane structures in solution (polymersomes) are found in various systems [39,40]. In solutions of crew-cut amphiphilic polymers, Eisenberg and co-workers have determined an entire wonderland of structures [41]. Some exhibit onion phases, while others are bicontinuous. The raspberry droplets with the inverted micelles (Fig. 9e) resemble so-called Large Compound Vesicles. The agreement at this point is qualitative, in particular regarding the difficult question of whether such systems are in local or global equilibrium—the answer depends on the actual formation process. Eisenberg prepares his systems by a very slow quench from good solvent,

with demonstrated exchange between different aggregates through fission and fusion phenomena [39]. The recently discovered high-genus giant superstructures ($\gg 1\,\mu m$) [42] have a striking resemblance to the bicontinuous droplets. But in our case the pores have size of the polymer coil, whereas in the superstructures the domains are apparently much larger than the constituting polymers. A more detailed comparison, using realistic experimental parameters, and calculation of the optimal droplet structure in an open system, is in progress; marvellous structures abound.

## CONCLUSION

The dynamical mean field approach is a powerful tool to predict and analyse block copolymer morphologies in a variety of systems. Extensions in further directions are pursued in our group and elsewhere: the development of a proper rheological model, the development of models for stiff-flexible polymer morphologies, charged systems and reactive systems. All these extensions can be treated to some extent at the mean field level. What remains a challenge for the foreseeable future however, is the prediction of morphologies in the case that specific interactions dominate, such as packing factors in rigid molecules, or hydrogen-bonding. Such factors are important when one considers molecular systems of biological origin, or in supramolecular chemistry.



### *Acknowledgements*

We thank Gerhard Goldbeck-Wood for many stimulating discussions.

### *References*

[1] Hamley, I.W. (1998) *The Physics of Block Copolymers* (Oxford University Press, Oxford).
[2] Fraaije, J.G.E.M. (1993) "Dynamic density-functional theory for microphase separation kinetics of block-copolymer melts", *J. Chem. Phys.* **99**, 9202–9212.
[3] Fraaije, J.G.E.M., van Vlimmeren, B.A.C., Maurits, N.M., Postma, M., Evers, O.A., Hoffmann, C., Altevogt, P. and Goldbeck-Wood, G. (1997) "The dynamic mean-field density functional method and its application to the mesoscopic dynamics of quenched block copolymer melts", *J. Chem. Phys.* **106**, 4260–4269.
[4] de Gennes, P.-G. (1979) *Scaling Concepts in Polymer Physics* (Cornell University, Ithaca, NY).
[5] Doi, M. and Edwards, S.F. (1986) *The Theory of Polymer Dynamics* (Clarendon, Oxford).
[6] Fredrickson, G.H., Ganesan, V. and Drolet, F. (2002) "Field-theoretic computer simulation methods for polymers and complex fluids", *Macromolecules* **35**, 16–39.
[7] Hill, T. (1962) *An Introduction to Statistical Thermodynamics* (Addison-Wesley, Reading).
[8] Flory, P.J. (1953) *Principles of Polymer Chemistry* (Cornell, Ithaca, NY).
[9] Flory, P.J. (1969) *The Statistical Mechanics of Chain Molecules* (Wiley, New York).
[10] Alexandridis, P., Lindmann, B., eds, (2000) *Amphiphilic Block Copolymers, Self-assembly and Applications* (Elsevier, Amsterdam).
[11] Leibler, L. (1980) "Theory of macroscopic separation in block copolymers", *Macromolecules* **13**, 1602–1617.
[12] Fleer, G.J., Cohen Stuart, M.A., Scheutjens, J.M.H.M., Cosgrove, T. and Vincent, B. (1993) *Polymers at Interfaces* (Chapman Hall, London).
[13] Szleifer, I., Benshaul, A. and Gelbart, W. (1990) "Chain packing statistics and thermodynamics of amphiphile monolayers", *J. Chem. Phys.* **94**, 5081–5089.
[14] Doi, M. (1996) *Introduction to Polymer Physics* (Clarendon Press, Oxford).
[15] Helfand, E. (1975) "Theory of inhomogeneous polymers: fundamentals of the Gaussian random-walk model", *J. Chem. Phys.* **62**, 999–1005.
[16] Helfand, E. and Wasserman, Z.R. (1976) "Block copolymer theory. 4. Narrow interface approximation", *Macromolecules* **9**, 879–888.
[17] Helfand, E. and Tagami, Y. (1996) "Theory of the interface between immiscible polymers", *J. Polym. Sci. B—Polym. Phys.*, 1947–1952, (Reprinted from *J. Polym. Sci. Polym. Lett.* (**9**) (1971) 741–746).
[18] Sevink, G.J.A., Zvelindovsky, A.V., van Vlimmeren, B.A.C., Maurits, N.M. and Fraaije, J.G.E.M. (1999) "Dynamics of surface directed mesophase formation in block copolymer melts", *J. Chem. Phys.* **110**, 2250–2256.
[19] Lyakhova, K.S., Zvelindovsky, A.V., Sevink, G.J.A. and Fraaije, J.G.E.M. (2003) "Inverse mapping of block copolymer morphologies", *J. Chem. Phys.* **118**, 8456–8459.
[20] Hamm, M., Goldbeck-Wood, G., Zvelindovsky, A.V. and Fraaije, J.G.E.M. (2003) "Microstructure of nematic amorphous block copolymers: dependence on the nematic volume fraction", *J. Chem. Phys.* **118**, 9401–9419.
[21] Maurits, N.M. and Fraaije, J.G.E.M. (1997) "Mesoscopic dynamics of copolymer melts: from density dynamics to external potential dynamics using nonlocal kinetic coupling", *J. Chem. Phys.* **107**, 5879–5889.
[22] Kawasaki, K. and Sekimoto, K. (1989) "Concentration dynamics in polymer blends and block copolymer melts", *Macromolecules* **22**, 3063–3075.
[23] Gardiner, C.W. (1990) *Handbook of Stochastic Methods*, 2nd Ed. (Springer, Berlin).
[24] van Vlimmeren, B.A.C., Maurits, N.M., Zvelindovsky, A.V., Sevink, G.J.A. and Fraaije, J.G.E.M. (1999) "Simulation of 3D mesoscale structure formation in concentrated aqueous solution of the triblock polymer surfactants (ethylene oxide) (13) (propylene oxide) (30) (ethylene oxide) (13) and (propylene oxide) (19) (ethylene oxide) (33) (propylene oxide) (19). Application of dynamic mean-field density functional theory", *Macromolecules* **32**, 646–656.
[25] Alexandridis, P. and Hatton, T.A. (1995) "Poly(ethylene oxide)–poly(propylene oxide)–poly(ethylene oxide) block-copolymer surfactants in aqueous solutions and at interfaces—thermodynamics, structure, dynamics and modeling", *Colloid Surface A* **96**, 1–46.
[26] Alexandridis, P., Olsson, U. and Lindmann, B. (1995) "Self-Assembly of amphiphilic block-copolymers—the (EO) (13) (PO) (30) (EO) (13)-water-*p*-xylene system", *Macromolecules* **28**, 7700–7710.
[27] Alexandridis, P., Olsson, U. and Lindmann, B. (1996) "Phase behavior of amphiphilic block copolymers in water-oil mixtures: the pluronic 25R4-water-*p*-xylene system", *J. Phys. Chem.* **100**, 280–288.
[28] Malcolm, N.M. and Rowlinson, J.S. (1957) "Thermodynamic properties of aqueous solutions of polyethylene glycol, polypropylene glycol and dioxane, Trans", *Faraday Soc.* **53**, 921–931.
[29] Dormidontova, E. (2002) "Role of competitive PEO–water and water–water hydrogen bonding in aqueous solution PEO behavior", *Macromolecules* **35**, 987–1001.
[30] Hamley, I.W., Castelletto, V., Yang, Z., Price, C. and Booth, C. (2001) "Melt phase behavior of poly(oxyethylene)–poly (oxypropylene) diblock copolymers", *Macromolecules* **34**, 4079–4081.
[31] Krevelen, D.W. (1990) *Properties of Polymers, Their Correlation with Chemical Structure. Their Numerical Estimation and*

*Prediction from Additive Group Contribution* (Elsevier, Amsterdam).
[32] Zvelindovsky, A.V.M., van Vlimmeren, B.A.C., Sevink, G.J.A., Maurits, N.M. and Fraaije, J.G.E.M. (1998) "Three-dimensional simulation of hexagonal phase of a specific polymer system under shear: the dynamic density functional approach", *J. Chem. Phys.* **109**, 8751–8754.
[33] Schmidt, G., Richtering, W., Lindner, P. and Alexandridis, P. (1998) "Shear orientation of a hexagonal lyotropic triblock copolymer phase as probed by flow birefringence and small-angle light and neutron scattering", *Macromolecules* **31**, 2293–2298.
[34] Hadziioannou, G., Mathis, A. and Skoulios, A. (1979) "Monocristaux de copolymers trisequences styrene/isoprene/styrene presentant la structure cylindrique: I Etude de l'orientation par diffraction des rayons X aux petits angles", *Colloid Polym. Sci.* **257**, 15.
[35] Matsen, M.W. and Schick, M. (1994) "Stable and unstable phases of a diblock copolymer melt", *Phys. Rev. Lett.* **72**, 2660–2663.
[36] Knoll, A., Horvat, A., Lyakhova, K.S., Krausch, G., Sevink, G.J.A., Zvelindovsky, A.V. and Magerle, R. (2002) "Phase behavior in thin films of cylinder-forming block copolymers", *Phys. Rev. Lett.* **89**, 035501.
[37] Fraaije, J.G.E.M. and Sevink, G.J.A. (2003) "Model for pattern formation in polymer surfactant nanodroplets", *Macromolecules* **36**, 7891–7893.
[38] Huinink, H.P., van Dijk, M.A., Brokken-Zijp, J.C.M. and Sevink, G.J.A. (2001) "Surface-induced transitions in thin films of asymmetric diblock copolymers", *Macromolecules* **34**, 5325.
[39] Discher, D.E. and Eisenberg, A. (2002) "Polymer vesicles", *Science* **297**, 967.
[40] Discher, B.M., Won, Y.Y., Ege, D.S., Lee, J.C.M., Bates, F.S., Discher, D.E. and Hammer, D.A. (1999) "Polymersomes: tough vesicles made from diblock copolymers", *Science* **284**, 1143.
[41] Cameron, N.S., Corbiere, M.K. and Eisenberg, A. (1999) "1998 E.W.R. Steacie Award Lecture asymmetric amphiphilic block copolymers in solution: a morphological wonderland", *Can. J. Chem.* **77**, 1311.
[42] Haluska, C.K., Góźdź, W.J., Döbereinder, H.-G., Förster, S. and Gompper, G. (2002) "Giant hexagonal superstructures in diblock-copolymer membranes", *Phys. Rev. Lett.* **89**, 238302.